Chin. J. Astron. Astrophys. Vol. 5 (2005), No. 5, 495–507
(*http://www.chjaa.org*)

Chinese Journal of
Astronomy and
Astrophysics

Autoregressive Spectral Estimation for Quasi-Periodic Oscillations *

Li Chen[1] and Ti-Pei Li[2,3]

[1] Department of Astronomy, Beijing Normal University, Beijing 100875; *chenli@bnu.edu.cn*
[2] Center for Astrophysics, Tsinghua University, Beijing 100084
[3] Key Lab. of Particle Astrophysics, Inst. of High Energy Physics, Chinese Academy of Sciences, Beijing 100039

Abstract Modern methods of spectral estimation based on parametric time-series models are useful tools in power spectral analysis. We apply the autoregressive (AR) model to study quasi-periodic oscillations (QPOs). An empirical formula to estimate the expectation and standard deviation of the noise AR power densities is derived, which can be used to estimate the statistical significance of an apparent QPO peak in an AR spectrum. An iterative adding-noise algorithm in AR spectral analysis is proposed and applied to studying QPOs in the X-ray binary Cir X-1.

Key words: methods: data analysis — stars: individual (Circinus X-1) — X-rays: stars

1 INTRODUCTION

Quasi-periodic oscillation (QPO) is a very common feature of accreting systems around compact objects. The history of finding the QPO phenomena of low-mass X-ray binaries (LMXBs) can be traced back to the early 70s. Angel et al. (1971) first reported that the X-ray of Sco X-1 has a 1–10 Hz oscillation. Tawaira et al. (1982) found that there was a 2 Hz pulse in rapid burst sources. These findings, however, did not attract much attention until the discovery of the 20–30 Hz QPOs by van der Klis et al. (1986) in the typical bright galactic bulge source GX 5-1 and the link of QPOs with millisecond pulsars suggested by them. QPOs have since been found in several LMXBs. After the launch of Rossi X-Ray Timing Explorer (RXTE) into orbit in Dec. 1995, its remarkable design of large area and high time resolution pushed the upper limit of frequency of QPOs in LMXBs to the kilohertz range. The sources 4U 1728-34 and Sco X-1 are the earliest ones found with kHz QPOs, with central frequencies at 800 Hz and 1100 Hz respectively (Strohmayer et al. 1996; van der Klis et al. 1996). Connecting such a high frequency with the Kepler time scale of the accretion disk at $r = 100$ km, by $\tau_{\rm dyn} = (r^3/GM)^{1/2} \sim 2$ ms, it is seen that the source originates from the neutron star (van der Klis 1997). Until recently,

* Supported by the National Natural Science Foundation of China and by the State Basic Science Research Projects of China.

13 sources show millisecond oscillations during thermonuclear X-ray bursts (see Muno 2004, for a review). More than 20 sources have shown kHz QPOs and some of them show twin kHz peaks (van der Klis 2000 for a review). The distribution of frequency is multi-peaked (Belloni et al. 2005). Although not as commonly as in LMXBs, pairs of 30–450 Hz QPOs have also been found in a few black hole candidates and their frequencies tends to appear in certain ratios (2:3, or 3:5) (Strohmayer 2001; Remillard et al. 2002; Abramowicz et al. 2003). By studying the rapid QPOs, we may obtain information on such topics as the strong field effect of general relativity theory and the state equation of compact objects. For example, QPOs with a central frequency of 67 Hz and 300 Hz have been observed in GRO 1915+105 and GRO J1655–40, respectively, which are the only known super-luminosity jet sources in the Galaxy (Morgen, Remillard & Greiner 1996; Remillard et al. 1996). If these QPOs are induced by the accretion disk precession frequency caused by frame dragging, it may suggest that there is a rapid rotational black hole in these two sources. The value of angular movement can be used to classify the black holes (Zhang, Cui & Chen 1997). Therefore, the detection of QPOs in X-ray sources is important for establishing or verifying astrophysical theories. Also, some Chinese astronomers are interested in the work in this field(cf. Wu 2005; Qian & Wu 2005).

The classical spectral estimation based on digital Fourier transform has been widely used in studying QPOs (Leahy et al. 1983; van der Klis 1988). Shortcomings exist in this method when applied to observed time series, e.g., the serious noise effect for long datasets and window effect for short datasets. It is to overcome these shortcomings that modern spectral estimation methods have been developed based on parametric models of stochastic process. We have found that power density spectrum in the autoregressive model (AR PDS) can better reveal the QPO peaks in Cyg X-1 (Chen, Feng & Li 2000; Chen et al. 2000). In Section 2 we compare the AR PDS and Fourier PDS of the same time series with known QPO components and with simulated white noise. Based on the good ability of AR PDS to reveal QPO peaks from noisy data shown by our simulation studies, an iterative adding-noise algorithm is proposed for studying QPOs in observed data. We examine the probability distribution of the noise AR power densities with Monte Carlo simulations and derive an empirical formula for its parameters in Section 3. An application of the AR spectral analysis technique to the X-ray source Circinus X-1 and a brief discussion are given in Section 4.

2 PDS OF SIMULATED DATA WITH KNOWN QPOS

2.1 AR(p) Model and Its Parameters

Let $\epsilon(i), i = 0, \pm1, \pm2, \cdots$ be a white noise process with zero mean and variance σ_ϵ^2 and $a(0), a(1), \cdots, a(p)$ be a set of real constants with $a(0) = 1$ and $a(p) \neq 0$. Then if $x(j)$ is a weakly stationary process which satisfies the different equation

$$\sum_{i=0}^{p} a(i)x(j-i) = \epsilon(j)\,, \qquad j = 0, \pm1, \pm2, \cdots\,, \tag{1}$$

and for which $\langle x(i)\epsilon(j)\rangle = 0$ for all $i \leq j-1, j = 0, \pm1, \pm2, \cdots$ then $x(j)$ is said to be an autoregressive process, denoted by AR(p). The number p is called the order of the autoregression (Koopmans 1974). From Eq. (1) and that $\langle \epsilon(j)x(j-l)\rangle = 0$ for $l = 1, 2, \cdots, p$, we obtain

$$\langle x(j)x(j-l)\rangle = -\sum_{i=1}^{p} a(i)\langle x(j-l)x(j-i)\rangle\,, \qquad l = 1, 2, \cdots, p\,. \tag{2}$$

However, by stationarity of x, $\langle (x(j) - \langle x\rangle)(x(j+k) - \langle x\rangle)\rangle$ only depends on the distance k, normalize $\langle x\rangle$ to zero, we define the auto covariance function as $r(k) \equiv \langle x(j)x(j+k)\rangle$.

Apparently, $\langle x(j-l)x(j-i)\rangle = r(l-i)$. Thus, Eq. (2) becomes

$$\sum_{i=1}^{p} c(i)r(l-i) = r(l)\,, \qquad l = 1, 2, \cdots, p\,, \tag{3}$$

where $c(i) = -a(i), i = 1, 2, \cdots, p$. These are the Yule-Walker Equations.

We have

$$\sigma_\epsilon^2 = \langle x(j) - \sum_{i=1}^{p} c(i)x(j-i)\rangle^2 = r(0) - 2\sum_{i=1}^{p} c(i)r(i) + \sum_{i,j=1}^{p} c(i)c(j)r(j-i)\,.$$

From Eq. (3), the above expression can be simplified to

$$\sigma_\epsilon^2 = r(0) - \sum_{i=1}^{p} c(i)r(i)\,. \tag{4}$$

In practice, $r(j)$ can be replaced by its unbiased estimator,

$$\hat{r} = \frac{1}{N-j}\sum_{k=1}^{N-j} x(k)x(k+j)\,,$$

where N is the sample size.

2.2 The PDS of AR(p) Process

The PDS of a series $x(k), P(f)$ is defined by the Fourier transform of its covariance $r(k)$:

$$P(f) = \frac{1}{2\pi}\sum_{k=-\infty}^{\infty} r(k)e^{-i2\pi k f\Delta t}\,.$$

There are different ways to determine $P(f)$. We view the problem from the angle of linear filtering. In an AR(p) model, the white noise $\epsilon(i)$ can be thought of as the output of a linear filter with, $x(i), x(i-1), \cdots, x(i-p)$ as the input, and $c(0) = 1, c(1), \cdots, c(p)$ are the filter coefficients. With the z-transform ($z = e^{i2\pi f\Delta t}$), we have

$$(1 - \sum_{j=1}^{p} c(j)z^{-j})X(z) = E(z)\,,$$

where $X(z)$ and $E(z)$ are the z-transform of the series $x(j)$ and $\epsilon(j)$, respectively. Thus, the frequency response of the AR(p) model is

$$C(z) = \frac{E(z)}{X(z)} = \frac{1}{1 - \sum_{j=1}^{p} c(j)z^{-j}}\,.$$

However, the spectral density functions of the input, $P_x(z)$, and of the output, $P_\epsilon(z)$, are related by the expression $P_x(z) = |C(z)|^2 P_\epsilon(z)$ (Jenkins & Watts 1968). Remember that $P_\epsilon(z)$ is the PDS of the white noise ϵ, that is, $P_\epsilon(z) = \sigma_\epsilon^2$. Replace z with $e^{i2\pi f\Delta t}$, we see that the AR(p) process has a continuous spectrum with spectral density of the form

$$P_x(e^{i2\pi f\Delta t}) = \frac{\sigma_\epsilon^2}{|1 - \sum_{j=1}^{p} c(j)e^{-i2\pi j f\Delta t}|^2} \equiv P(f)\,, \tag{5}$$

where f(Hz) is the frequency. We label the PDS given in Eq. (5) as AR PDS.

2.3 Determining the Value of Order p

Equation (5) is quite sensitive to p. If p is too small, the QPO frequency will be shifted severely or even the QPO peak can not be found at all. A larger value of p may bring a higher spectral resolution, but too large p will cause the peak to split and produce many pseudo-peaks in the AR PDS. Some usually used criterions to determine the value of p are as follows:

(1) *FPE (Final prediction error) criterion* (Akaike 1970). According to FPE, p takes the value where the function

$$\mathrm{FPE}(p) = \frac{1+p/N}{1-p/N}\sigma_\epsilon^2(p)$$

reaches its minimum. Here N= sample size, $1 \le p \le N/10$, $\sigma_\epsilon^2(p) = r(0) - \sum_{i=1}^{p} c(i)r(i)$.

(2) *AIC (A-Information Criterion)* (Akaike 1973). Let

$$\mathrm{AIC}(k) = \ln \sigma_\epsilon^2(k) + 2k/N\,,$$

where $k = 1, 2, \cdots, L$, L is a few times $\ln N$. Then $p = k|_{\mathrm{AIC}(k)=\min}$.

(3) *CAT (Autoregressive transfer function criterion)* (Parzen 1976),

$$\mathrm{CAT}(k) = \frac{1}{N}\sum_{j=1}^{k}\frac{N-j}{N\sigma_\epsilon^2(j)} - \frac{N-k}{N\sigma_\epsilon^2(k)}\,.$$

where $p = k|_{\mathrm{CAT}(k)=\min}$.

There are also other criterions that are commonly used. However, all, including those listed above, usually give underestimates of p in practice.

2.4 QPO Model

The AR(2) model,

$$x(i) = c(1)x(i-1) + c(2)x(i-2) + \epsilon(i)\,, \quad \epsilon(i) \sim N(0, \sigma_\epsilon^2)\,, \tag{6}$$

where $N(\mu, \sigma_\epsilon^2)$ is a normal distribution with expectation μ and standard deviation σ_ϵ, which may contain a QPO in its PDS with a peak at

$$f_c = [\cos^{-1}(c(1)(1-c(2))/4|c(2)|)/2\pi]/\Delta t \quad (\mathrm{Hz}), \tag{7}$$

under the condition that $c(2) < 0$ and $|c(1)(1-c(2))/4c(2)| < 1$ (Priestley 1981). With $\Delta t = 1/64\,\mathrm{s}$ time bin, we make two AR(2) series

$$u(i) = 1.6u(i-1) - 0.9u(i-2) + \eta(i), \tag{8}$$

and

$$v(i) = 0.5v(i-1) - 0.9v(i-2) + 5\zeta(i)\,, \tag{9}$$

where $\eta(i) \sim N(0,1)$ and $\zeta(i) \sim N(0,1)$ are two independent white noises. The expected PDS of $u(i)$ and $v(i)$ calculated by Eq. (5) are presented in Figure 1. From Eq. (7) $u(i)$ has a QPO at 5.76 Hz in its PDS (peak 1 in Fig.1) and $v(i)$ has one at 13.28 Hz (peak 2 in Fig.1). Adding these two series up, we obtain a series $x(i) = u(i) + v(i)$ with two QPO components. Because the two series are independent, the PDS of $x(i)$ is the simple sum of the two spectra of $u(i)$ and $v(i)$ (see Fig.1). We produce a sample of $x(i)$ for i from 1 to 40960 (the sample interval $T = 640$ s) from the models (8) and (9) with the initial values $u(0) = u(1) = v(0) = v(1) = 0$. Using a linear transform $x' = (x - \overline{x})/\sigma(x) + 1$ we can obtain a new sequence with both mean

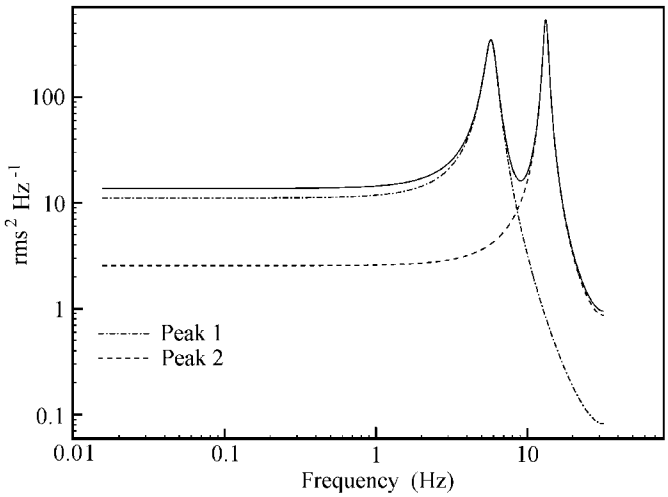

Fig. 1 Power density spectra of QPO models. *Dashed line*: PDS of the model (8) with a QPO peak at ∼5.76 Hz. *Dot-Dashed line*: PDS of model (9) with a QPO peak at ∼ 13.28 Hz. *Solid line*: PDS of the model (8)+(9) with two QPO components.

and variance being unity. We still denote the normalized sequence as $x(i)$. To compare the AR and Fourier spectral estimations on the ability of extracting QPOs from noisy data, we add an additional noise component $a \cdot \epsilon(i)$ on the same $x(i)$ produced above

$$y(i) = x(i) + a \cdot \epsilon(i)\,, \qquad \epsilon \sim N(1,1)\,, \tag{10}$$

where a takes the values 0, 10, 30 or 50 in turn.

As is usual with PDS obtained with FFT, each produced sample of $y(i)$ is divided into 10 64-second segments. A 4096-point FFT and spectral estimation of AR model with order $p = 25$ are performed on each segment to obtain Fourier PDS, $P_F(f)$, and AR PDS, $P_{\rm AR}(f)$, respectively. Taking the average of these PDSs, we acquire the PDS with the error-bar

$$\mathrm{err}(f) = \sqrt{\frac{\sum_{k=1}^{10}(P_k(f) - \overline{P}(f))^2}{10(10-1)}}$$

at f(Hz). To compare the significance of the spectral components, all spectra are normalized to the one with mean=3 (so that all data including their error-bars are kept positive) and variance=1. Finally, all spectra are logarithmically rebinned to reduce the scatter at high frequencies. The FFT PDS and AR PDS are respectively shown in the top and middle rows of Figure 2.

We use a constant pulsing Gaussian curve

$$P(f) = A + \frac{B_1}{w_1\sqrt{\pi/2}} \exp\Big(-2\Big(\frac{f-f_{c1}}{w_1}\Big)^2\Big) + \frac{B_2}{w_2\sqrt{\pi/2}} \exp\Big(-2\Big(\frac{f-f_{c2}}{w_2}\Big)^2\Big)$$

to fit the PDS. Because each PDS is normalized to standard deviation=1, we can define the signal significance at the $i^{\rm th}$ central frequency f_{ci}(Hz)$(i = 1, 2)$ by $S(f_{ci}) = ((P(f_{ci}) - P(background))/\mathrm{STD}(P(f))$. Here $P(f_{ci}) - P(background) = B_i/(w_i\sqrt{\pi/2})$ is the height of

Table 1 QPO locations in Fourier, AR and AN-AR spectra for simulated data with two known QPO components

		Peak 1 (5.76 Hz)		Peak 2 (13.28 Hz)	
	a	f_{c1} (Hz)	Significance	f_{c2}(Hz)	Significance
FFT	0	5.76±0.03	2.4±0.3	13.27±0.01	6.8±0.4
	10	5.77±0.11	2.0±1.1	13.24±0.05	5.9±1.4
	30	5.93±0.33	1.2±1.3	13.13±0.13	3.6±1.8
	50	–	–	13.22±0.42	1.4±3.2
AR	0	5.74±0.02	2.4±0.2	13.28±0.01	6.6±0.3
	10	5.58±0.08	1.7±0.4	13.30±0.03	6.1±0.6
	30	6.78±0.28	1.5±0.9	13.28±0.13	3.9±1.1
	50	–	–	12.57±0.35	2.0±2.3
AN-AR	0	5.74±0.02	2.3±0.2	13.28±0.01	6.6±0.2
	10	5.57±0.04	2.1±0.3	13.22±0.02	6.2±0.4
	30	5.98±0.11	1.9±0.4	13.19±0.05	5.2±0.7
	50	6.16±0.15	1.8±0.8	13.30±0.08	4.8±1.0

the Gaussian peak; $\mathrm{STD}(P(f)) = 1$, is the standard deviation. The QPO characteristics determined from the Fourier and AR PDS are presented in the upper two boxes in Table 1.

Based on the ability of AR spectral estimation to extract QPO signal from noise-dominated data, an iterative adding-noise algorithm can be proposed: repeatedly produce K length T samples of $z(i)$ by

$$z(i) = y(i) + \eta(i)\,, \qquad \eta \sim N(\lambda, \lambda)\,, \tag{11}$$

where λ is the mean of series $y(i)$.Calculate AR PDS for the K samples separately, take the average of the K spectra as the final result and denote it by AN-AR PDS. With $K = 100$ we draw the AN-AR PDS from the 100 samples of $z(i)$ and show the results in the bottom of Figure 2 and Table 1.

From Figure 2 and Table 1 we can see that compared to the Fourier technique, the AN-AR spectral estimation is better able to extract QPOs from noisy data. When $a = 30$ and 50 in the FFT spectra, we can hardly find the QPO at 5.76 Hz, and the significance of the component near 13 Hz is small, too. When the background noise increases, the signal significance of Fourier power spectrum decreases quickly, but there always exist remarkable QPOs in the AN-AR PDS. In the case of $a = 50$ where the additional noise is 50 times the original signal $x(i)$, both the Fourier spectra and the AR PDS have almost completely lost the QPOs but the AN-AR PDS still shows them clearly. It is easy to see that the QPO components are clearer and the pseudo peaks are much smaller in AN-AR PDS than that in normal AR PDS. We chose different values of p between 25–40 to calculate AN-AR PDS, the results near 13.28 Hz are hardly affected, but there would be a ∼0.5 Hz frequency shift around 5.76 Hz.

3 THE PROBABILITY DISTRIBUTION OF THE NOISE AR POWER DENSITIES

To estimate the statistical significance of detecting a QPO peak in a power density spectrum against a background of noise, we need to know the probability distribution of the noise power densities in a PDS of data of pure noise. We study the distribution of the noise AR power

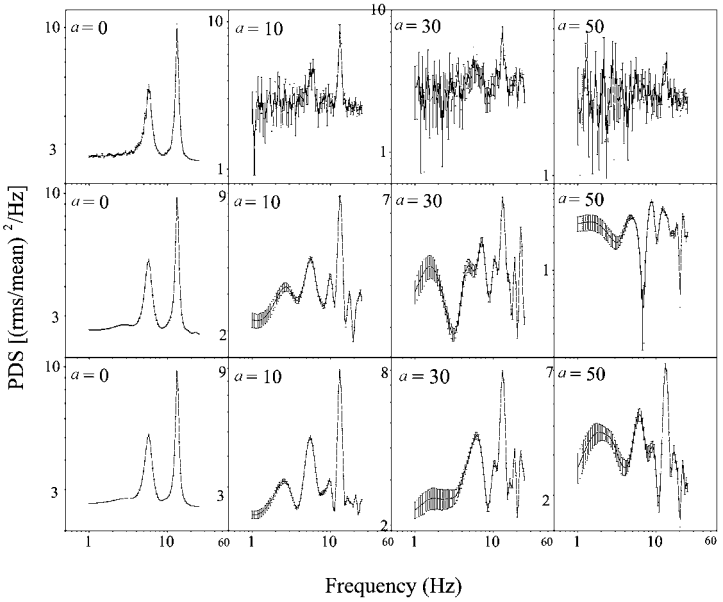

Fig. 2 Power density spectra for different noise component added to the same simulated data of the model (8)+(9). The analyzed data for each spectrum are produced by $y(i) = x(i) + a \cdot \eta(i)$, where $x(i)$ is a normalized sample of the model (8)+(9), $\eta(i) \sim N(1,1)$. Each PDS is normalized to mean=3 and standard deviation=1. *Top row*: Fourier spectra. *Middle row*: AR spectra with $p = 25$. *Bottom row*: AN-AR spectra with $p = 25$.

densities by a Monte Carlo approach. We produce 100 random samples of stochastic process of pure noise following the normal distribution $N(1,1)$. For each sample i $(i = 1, \cdots, 100)$ the average AR power densities $\overline{P}_i(f)$ with a AR(p) model $(p = 5, 10, 15, 20, 25, 30)$ are calculated from M data segment $(M = 1, 2, 4, 8, 16, 32, 64)$, with each segment containing N data points $(N = 512, 1024, 2048, 4096)$. For each parameter set (p, N, M) the noise AR power density $\overline{P}_i(f)$ $(i = 1, \cdots, 100)$ is tested by the Kolmogorov test to see whether they are normally distributed. The results show that for all parameter values the average noise power AR densities follow the normal distribution at the 95% confidence level.

For each given set of p, N and M, the mean $\mu = \sum_i \overline{P}_i/100$ and variance $s^2 = \sum_i (\overline{P}_i - \mu)^2/(100-1)$ are calculated. All the means are in the range of 1.00 ± 0.02, independent of the order p, data length N and segment number M. For each set (N, M) the quantity $\sqrt{p}$ varies linearly with s (see Fig. 3). The distribution of $\sqrt{MN/2}s$ vs $\sqrt{p}$ shown in Figure 4 can be fitted simply by a straight line

$$\sqrt{\frac{NM}{2}}s = (-0.175 \pm 0.028) + (1.055 \pm 0.007)\sqrt{p}\,. \tag{12}$$

Then, for a noise spectrum with length N, segment number M and order p of the AR model, we have an empirical estimate of its expectation and standard deviation:

$$\langle \overline{P} \rangle \;\approx\; 1\,,$$

$$\sigma_{\overline{P}} \in \left[\sqrt{\frac{2}{NM}}(1.04\sqrt{p} - 0.21),\ \sqrt{\frac{2}{NM}}(1.07\sqrt{p} - 0.14)\right]. \tag{13}$$

Here we always have $M > 1$ and $N \gg 1$. Therefore, in Eq. (13), when p is large enough (e.g. $p > 10$) the second term in each round bracket becomes negligible, thus

$$\sigma_{\overline{P}}^2 \approx \frac{2p}{NM} \,. \tag{14}$$

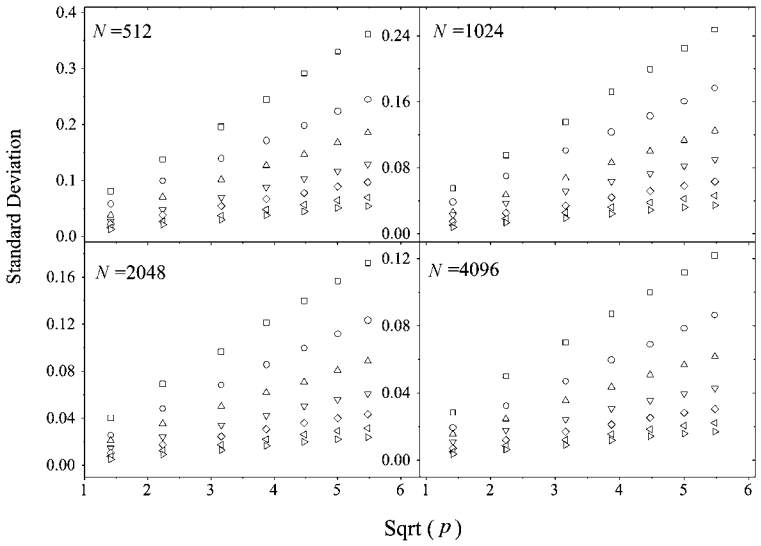

Fig. 3 Relations of the standard deviation s vs $\sqrt{p}$ for seven different values of data segment number M. The symbols of square, circle, up triangle, down triangle, diamond, left triangle and right triangle are correspondent to $M = 1, 2, 4, 8, 16, 32$ and 64, respectively. N denotes the number of points in each segment.

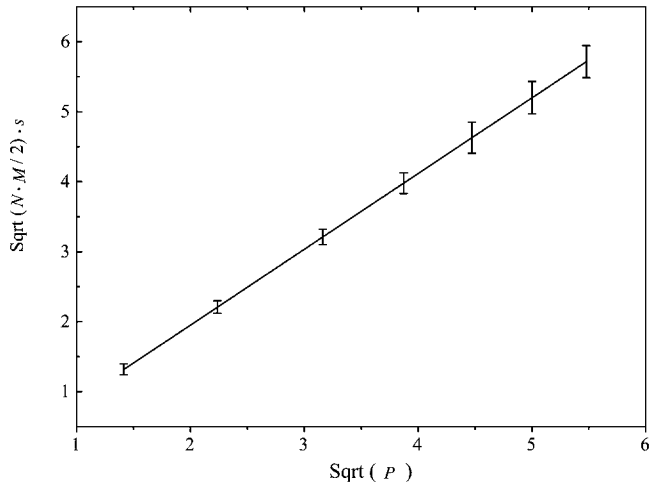

Fig. 4 Linear relation between $\sqrt{p}$ and reduced standard deviation $s\sqrt{MN/2}$. The error bars are the standard deviations of 28 values of $s\sqrt{MN/2}$ at each p.

Obviously, a noise spectrum of higher order, lower time resolution and shorter segment corresponds to a larger variance. In fact, the order p is determined by the intrinsic properties of the time series. For a given segment number $\sigma^2_{\overline{P}} \propto 1/N,\ \sigma^2_{\overline{P}} \to 0$ when $N \to \infty$, consistent with the theoretical spectrum of white noise.

4 APPLICATION AND DISCUSSION

We applied the AR spectral analysis method proposed above to study QPOs in the X-ray emission from Cir X-1. Cir X-1 is a low magnetic field neutron star (Tennant, Fabian & Shafer 1986). Some QPO peaks, ranging between 1.3 and 32 Hz, have been reported (Shirey et al. 1998 and Ref. in). We use the observational data of Cir X-1 taken with the Main Pointing Detector PCA (Proportional Counter Array) on board RXTE between 09:25′:20″ and 09:56′:06″ on 18/05/1997. The Single-Bit Mode PCA data in 2–13 keV band with a time resolution of 122 μs is used in our analysis. From the data, we select a span of 1664 s that is continuous without any observational gap. First, with $\Delta t = 1/64$ s time bin we calculate the average Fourier PDS from 26 segments, each segment has a length of 64 s ($M = 26,\ N = 4096$). Then we do the same thing to the noise-added series $y(i) = x(i) + a \cdot \epsilon(i)$, where $x(i)$ is the original data and $\epsilon(i) \sim N(\lambda, \lambda)$ with λ being the average counts during a time bin in each segment of data. Figure 5 displays the resulting Fourier spectra and AN-PDS for the unadulterated observational data ($a = 0$) and different noise-added data ($a = 10, 50, 100$), with $p = 26$ estimated by the FPE criterion ($\overline{p} = 11$). We use the following function,

$$P = A_1 + A_2 f + A_3 f^2 + \frac{B}{w\sqrt{\pi/2}} \exp\Big(-2\Big(\frac{f - f_c}{w}\Big)^2\Big) \tag{15}$$

to fit each PDS to find the QPO frequency f_c and w. The average Leahy-normalized Fourier power density approximately follows a normal distribution with mean 2 and standard error $2/\sqrt{M}$ (Leahy et al. 1983). The Fourier spectra in the paper is normalized to one half of the Leahy-normalized PDS, therefore, the mean=1 and the standard error = $(1/2)/\sqrt{M}$. The significance of QPO in the FFT PDS can be defined by $S = 2(\overline{P}_c - 1)/\sqrt{M}$, where $\overline{P}_c$ is the average power density at f_c. The significance of QPO in the average AR PDS is defined by $S = (\overline{P}_c - 1)/\sigma_{\overline{P}}$, where the $\sigma_{\overline{P}}$ is estimated by Eq. (14). Table 2 lists the QPO characteristics obtained by the Fourier and AN-AR spectra for different noise-added data.

Now we apply the proposed iterative adding-noise algorithm to analyze the observation data. A difficulty in the AR spectral analysis is how to determine the value of order p. Although some criteria for selecting p have been proposed (see Section 2.3), they usually result in an underestimate on p in practice. The iterative adding-noise algorithm can weaken the demand for accurate estimate of model order. As AR spectral analysis is able to extract weak QPO signal from noisy data, AN-AR PDS can still show QPOs as AR PDS does for the original data. However, as the artificially added noises are statistically independent from each other, pseudo peaks should be smoothed out in the final averaged AN-AR PDS from many ($K \gg 1$) noise-dominated data segments. One of the advantages of the iterative adding-noise algorithm is that even larger p would not cause peak splitting and we may obtain a good frequency resolution as well. To derive the adding-noise AR spectrum we took the time bin = 1/32 S and $p = 32$, The analyzed 1644 s duration is divided into $M = 13$ segments and each segment contains $N = 4096$ consecutive counts $x(i)$. For each segment 500 noise-added data $y(i) = x(i) + \epsilon(i)$ are produced by independently adding noise ϵ with the same average rate as the signal. The final AN-AR PDS is shown in Figure 6.

The obtained AN-AR PDS shows that besides the ∼12 Hz QPO there may exists another low frequency component in Cir X-1. We use Eq. (15) to fit the AN-AR PDS of Cir X-1 and find that $f_{c1} = 12.31 \pm 0.01$ Hz, $w_1 = 2.25 \pm 0.01$ Hz with fractional rms = $(4.1 \pm 0.4)\%$ and

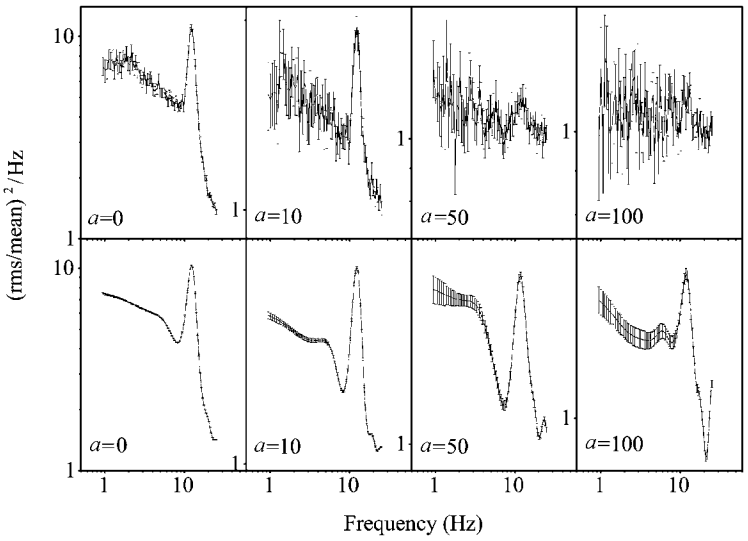

Fig. 5 Power spectra of X-rays from Cir X-1. *Upper row*: Fourier spectrum. The analyzed light curve is 1664 s long and the time step is 1/64 s. Each plotted spectrum is normalized to $0.5P_{\rm leahy}$ with an average of 26 spectra from 4096-point FFT for 64 s segments. An artificial noise $a \cdot \epsilon$, $\epsilon \sim N(\lambda, \lambda)$ is added on the data, where $\lambda = 244.407$ is the average counts in a time bin of observation data of Cir X-1. *Lower row*: AN-AR PDS with $p = 11$. The data are logarithmically rebinned to reduce scatter at high frequencies. Each plotted spectrum is normalized to $0.5P_{leahy}$ with an average of 13 spectra from 4096-point AR PDS for 128 s segments.

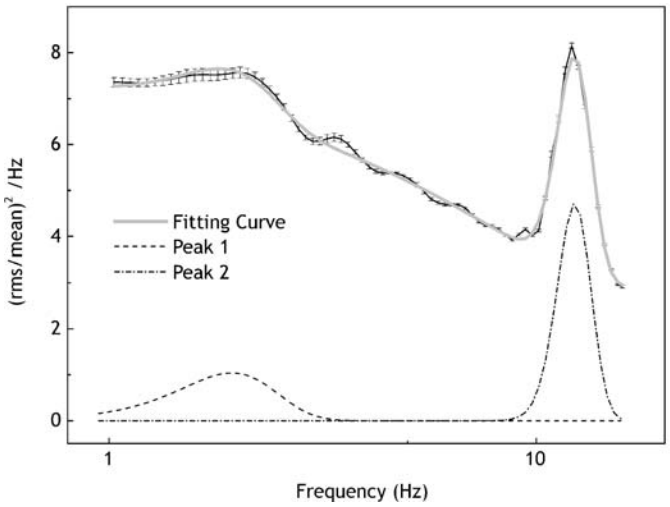

Fig. 6 AN-AR spectrum of Cir X-1. The spectrum is an average of 500 spectra from noise-added samples with Eq. (10), where $y(i) = x(i)$ and the used AR order $p = 32$. The data are logarithmically rebinned to reduce scatter at high frequencies. The spectrum is normalized to $0.5P_{\rm leahy}$ with an average of 13 spectra from 4096-point FFT for 64 s segments.

Table 2 QPO Parameters in Fourier and AR Spectra for Noise-added Data

		AR ($p = 11$)		
a	f_c (Hz)	w (Hz)	rms (%)	S
0	12.4 ± 0.01	2.90 ± 0.01	5.7 ± 0.4	245.0 ± 1.7
10	12.4 ± 0.01	2.98 ± 0.02	1.8 ± 0.4	23.1 ± 0.3
50	12.4 ± 0.03	4.23 ± 0.08	0.9 ± 0.1	4.0 ± 0.3
100	12.1 ± 0.05	4.25 ± 0.14	0.7 ± 0.2	2.4 ± 0.4
		Fourier		
a	f_c (Hz)	w (Hz)	rms (%)	S
0	12.4 ± 0.03	2.67 ± 0.05	5.5 ± 0.8	74.0 ± 3.0
10	12.4 ± 0.06	2.37 ± 0.06	1.7 ± 0.4	7.4 ± 0.9
50	12.5 ± 0.35	3.87 ± 0.93	0.9 ± 0.1	1.2 ± 0.7
100	12.0 ± 0.34	2.41 ± 0.79	0.6 ± 0.4	0.9 ± 0.6

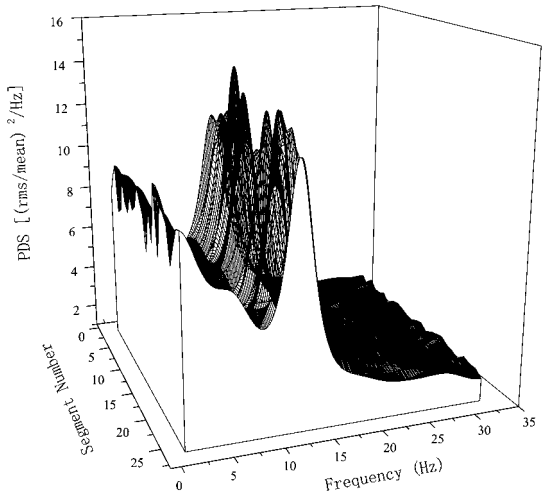

Fig. 7 Evolution of power spectrum of Cir X-1. Each curve is the AN-AR PDS of a 64 s segment which is an average of 500 spectra from noise-added samples with $a = 0$ and AR order $p = 11$. Error bars are not shown in the plot.

significance $S = 48.2 \pm 0.1$ for the normal QPO component. The second QPO component is at $f_{c2} = 1.94 \pm 0.02$ Hz with width $w_2 = 1.03 \pm 0.04$ Hz, rms $= (1.3 \pm 0.3)\%$ and S$=10.6 \pm 0.1$. Although the low frequency component might not be ranked as a QPO, it does look very significant!

Based on the high sensitivity of AR spectral analysis in revealing QPOs and the ability of the iterative AN-AR algorithm in depressing the effect of background noise, we can study the spectral evolution segment by segment. The process of adding noise on the same data of a segment for K times can produce K artificial noise-dominated segments which are almost independent samples. QPO peaks can show up in the AR PDS of each noise-added segment and then in the resultant average PDS, but, at the same time, the noise effect can be greatly

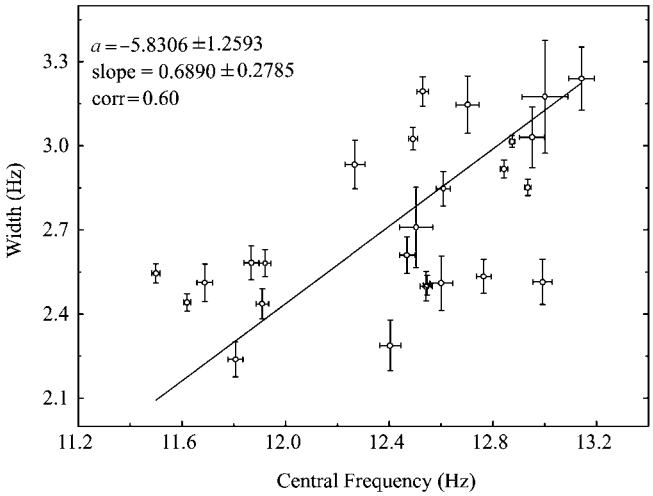

Fig. 8 Correlation between the central frequency and the width. The correlation coefficient between the central frequency and the width is ∼0.6.

depressed by averaging over the K spectra. The whole 26 AN-AR spectra ($p = 11$) of a single segment are displayed in Figure 7, from which we can see the evolution of QPO clearly at ∼12 Hz in Cir X-1 during the time analyzed. Using Eq. (15) to fit the QPO components in each segment, we find that there is some correlation between the central frequency and the width (Fig. 8), the correlation coefficient is ∼0.6.

Acknowledgements The authors acknowledge insightful suggestions by Prof. Mei Wu and Dr. Wenfei Yu. This work has been partially supported by the National Nature Science Foundation of China (Grant 10273010) and by the State Basic Science Research Projects of China (TG20000776), and made use of data obtained through the HEASARC online service, provided by the NASA/GSFC.

References

Abramowicz M. A., Bulik T. Bursa M. et al., 2003, A&A, 404, L21
Akaike H.,1970, Ann. Inst. Statist. Math., 22, 203
Akaike H., 1973, In: R. Flrtcher ed., Proc. 2nd Intern. Sym. on Information Theory, London: Academic Press, 13
Angel J. R. P., Kestenbaum H., Novick R., 1971, ApJ, 169, L57
Belloni T., Mendez M., Homan J., 2005, preprint(astro-ph/0501186)
Chen L., Feng Y. X., Li T. P. et al., 2000, Chin. Astron. Astrophys., 24, 159
Chen L., Li T. P., Song L. M. et al., 2000, Chin. Astron. Astrophys., 24, 297
Cooley J. W., Turkey J. W., 1965, Math. Comput., 19, 297
Jenkins G. M., Watts D. G.,1968, Spectral Analysis and its Application, San Francisco: Holden-Day
Koopmans L. H., 1974, The Spectral Analysis of Time Series, New York: Academic Press
Leahy D. A., Darbro W., Elsner R. F. et al., 1983, ApJ, 266, 160
Morgan E., Remillard R. A., Greiner J., 1996, IAUC, 6392
Moss F., Wiesenfeld K., 1995, Scientific American, August 53

Muno M. P., 2004, preprint(astro-ph/0403394)
Parzen E., 1976, In: Statistical Sci. Div., State Univ. of New York at Buffalo, Tech. Rep., 23
Priestly M. B., 1981, Spectral Analysis and Time Series, London: Academic Press
Qian L., Wu X. B., 2005, ChJAA, 5(s), 258
Remillard R. A., Morgan E. H., McClintock J. E., 1997, In: Texas Symposium on Relativistic Astrophysics, the Annals of the N. Y. Academy of Sciences, 750R
Remillard R. A., Muno M. P., McClintock J. E. et al., 2002, ApJ, 580, 1030
Shirey R. E., Bradt H. V., Levine A. M. et al., 1998, ApJ, 506, 374
Strohmayer T. E., Zhang W., Swank J. H. et al., 1996, ApJ, 469, L9
Strohmayer T. E., 2001, ApJ, 552, L49
Tawara Y., Hayakawa S., Hunieda H. et al., 1982, Nature, 299, 38
Tennant A. F., Fabian A. C., Shafer R. A., 1986, MNRAS, 221, 27
Wu X. B., 2005, ChJAA, 5(S), 235
van der Klis M., 1986, In: K. O. Mason, M. C. Watson, N. E. White, eds., The physics of Accretion onto Compact Objects, Lecture Notes in Physics, 266, 157
van der Klis M., 1988, In: Ogelmen E. P. J., van den Heuvel, eds., Timing Neutron Stars, Kluwer Academic Publishers, 27
van der Klis M., Swank J. H., Zhang W. et al., 1996, ApJ, 469, L1
van der Klis M., 1997, preprint (astro-ph/9710016)
van der Klis M., 2000, ARA&A, 38, 717
Wiesenfeld K., Moss F., 1995, Nature, 373, 33
Zhang S. N., Cui W., Chen W., 1997, ApJ, L155